iScience

CellPress
OPEN ACCESS

Article

Interleukin-34 Limits the Therapeutic Effects of Immune Checkpoint Blockade

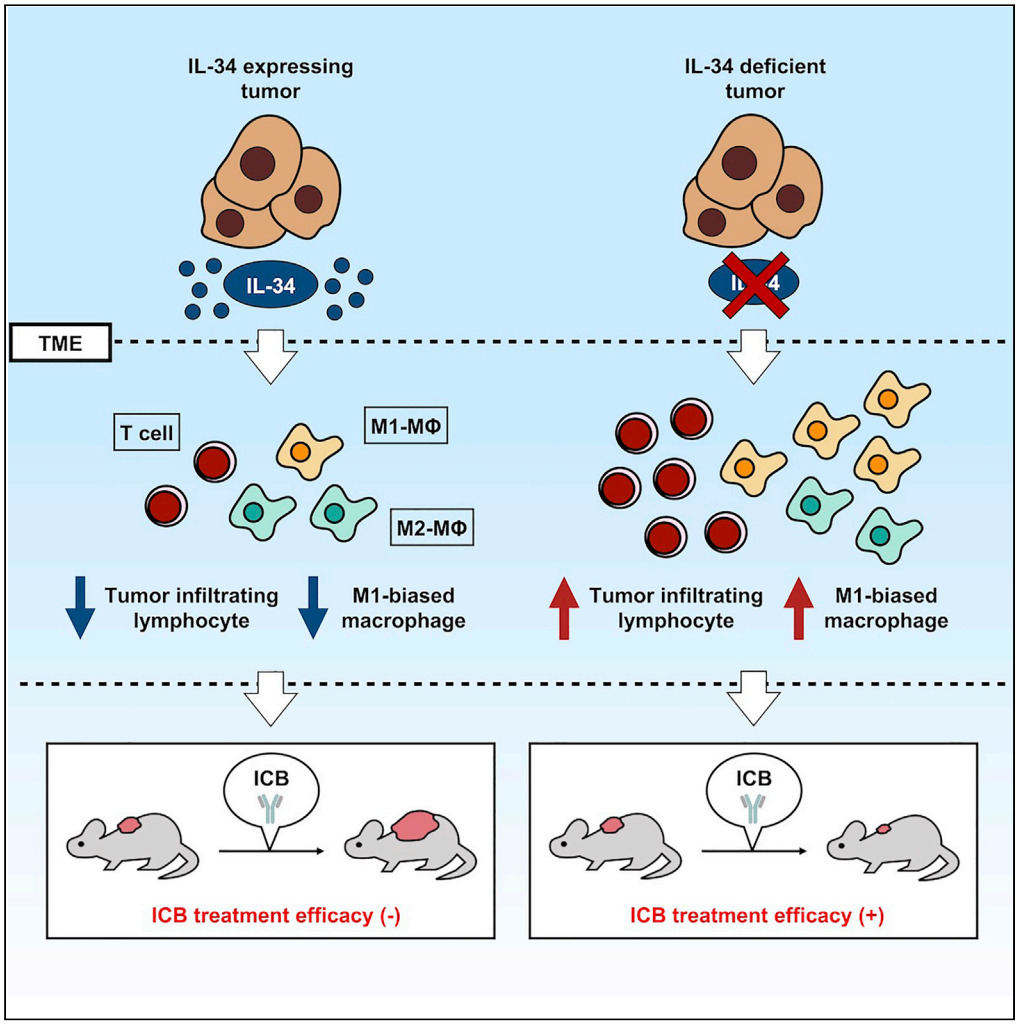

Naoki Hama, Takuto Kobayashi, Nanumi Han, ..., Hideo Yagita, Muhammad Baghdadi, Ken-ichiro Seino

seino@igm.hokudai.ac.jp

HIGHLIGHTS

IL-34-expressing tumors are resistant to ICB in several murine models

IL-34 upregulates the ratio of M2-biased to M1-biased macrophage in TME

Blockade of IL-34 with neutralizing antibody (Ab) enhances the efficacy of ICB

Anti-human IL-34 Ab shows the potential to enhance PD-1 blockade efficacy in PDX model

Hama et al., iScience 23, 101584
October 23, 2020
https://doi.org/10.1016/j.isci.2020.101584

iScience

CellPress
OPEN ACCESS

Article

Interleukin-34 Limits the Therapeutic Effects of Immune Checkpoint Blockade

Naoki Hama,[1,5] Takuto Kobayashi,[1,5] Nanumi Han,[1,5] Fumihito Kitagawa,[1] Nabeel Kajihara,[1] Ryo Otsuka,[1] Haruka Wada,[1] Hee-kyung Lee,[2] Hwanseok Rhee,[2] Yoshinori Hasegawa,[3] Hideo Yagita,[4] Muhammad Baghdadi,[1] and Ken-ichiro Seino[1,6,*]

SUMMARY

Interleukin-34 (IL-34) is an alternative ligand to colony-stimulating factor-1 (CSF-1) for the CSF-1 receptor that acts as a key regulator of monocyte/macrophage lineage. In this study, we show that tumor-derived IL-34 mediates resistance to immune checkpoint blockade regardless of CSF-1 existence in various murine cancer models. Consistent with its immunosuppressive characteristics, the expression of IL-34 in tumors correlates with decreased frequencies of cellular (such as $CD8^+$ and $CD4^+$ T cells and M1-biased macrophages) and molecular (including various cytokines and chemokines) effectors at the tumor microenvironment. Then, a neutralizing antibody against IL-34 improved the therapeutic effects of the immune checkpoint blockade in combinatorial therapeutic models, including a patient-derived xenograft model. Collectively, we revealed that tumor-derived IL-34 inhibits the efficacy of immune checkpoint blockade and proposed the utility of IL-34 blockade as a new strategy for cancer therapy.

INTRODUCTION

The immune checkpoint blockade (ICB) is an attractive approach to activate therapeutic antitumor activity (Cheng et al., 2018; Garon et al., 2015; Hodi et al., 2010). However, tumors frequently develop immune resistance against T cells that are specific for tumor antigens, resulting in limited therapeutic benefits in the clinic (Herbst et al., 2014; Hugo et al., 2016; Wang et al., 2017). Several studies have suggested multiple mechanisms of immune resistance at the molecular and cellular levels, such as impaired infiltration and activation of T cells at the tumor microenvironment (TME), epigenetic changes in tumor cells that lead to impaired interferon-gamma (IFNγ) signaling, and immunosuppression at the local TME (O'Donnell et al., 2017; Pardoll, 2012; Ribas, 2015). In this context, the enrichment of the TME with immunosuppressive cells such as M2-biased tumor-associated macrophages (TAMs), myeloid-derived suppressor cells (MDSCs), and regulatory T cells (Tregs) in addition to various metabolic and inflammatory mediators such as indoleamine 2,3-dioxygenase (IDO), arginase1 (ARG1), and prostaglandin E2 (PGE2) have been suggested to play critical roles in both innate and acquired resistance to immunotherapy (Kumar et al., 2016; Prima et al., 2017; Ugel et al., 2015). In many cases, the immunosuppressive TME is generated and continuously maintained by soluble factors secreted by the tumor cells (Binnewies et al., 2018). Accordingly, targeting these factors may help relieve immunosuppression and improve immunotherapeutic responses (Ghirelli and Hagemann, 2013; Pitt et al., 2016).

Among several therapeutic candidates, colony-stimulating factor-1 (CSF-1) receptor (CSF-1R) has gained much attention as a key molecule that controls the survival, proliferation, and functions of M2-biased TAMs with enhanced immunosuppressive activities (Noy and Pollard, 2014). Importantly, CSF-1/CSF-1R axis has been involved in promoting resistance to programmed death-1 (PD-1)/PD-L1 blockade, including, but not limited to, melanoma, hepatocellular carcinoma, and pancreatic cancer (Cannarile et al., 2017; Gyori et al., 2018; Neubert et al., 2018; Quaranta et al., 2018; Zhu et al., 2019). In addition to CSF-1, CSF-1R can be alternatively activated by binding with its second ligand, IL-34 (Lin et al., 2008). Although both of CSF-1 and IL-34 share the same receptor and show comparable effects on myeloid cells cultured *in vitro*, the two cytokines surprisingly show neither similar sequences nor common motifs and bind to distinct pockets within the extracellular domain of CSF-1R, resulting in different activation patterns of CSF-1R (Kim et al., 2006). A major difference between IL-34 and CSF-1 is the selective expression of

[1]Division of Immunobiology, Institute for Genetic Medicine, Hokkaido University, Kita-15 Nishi-7, Sapporo 060-0815, Japan

[2]DNA Link, Inc., Biomedical Science Building 117, Seoul National University College of Medicine, 103 Daehakro, Jongro-gu, Seoul 03080, South Korea

[3]Laboratory of Clinical Omics Research, Department of Applied Genomics, Kazusa DNA Research Institute, 2-6-7 Kazusa-kamatari, Kisarazu, Chiba 292-0818, Japan

[4]Department of Immunology, Juntendo University School of Medicine, 2-1-1 Hongo, Bunkyo-ku, Tokyo 113-8421, Japan

[5]These authors contributed equally

[6]Lead Contact

*Correspondence: seino@igm.hokudai.ac.jp

https://doi.org/10.1016/j.isci.2020.101584

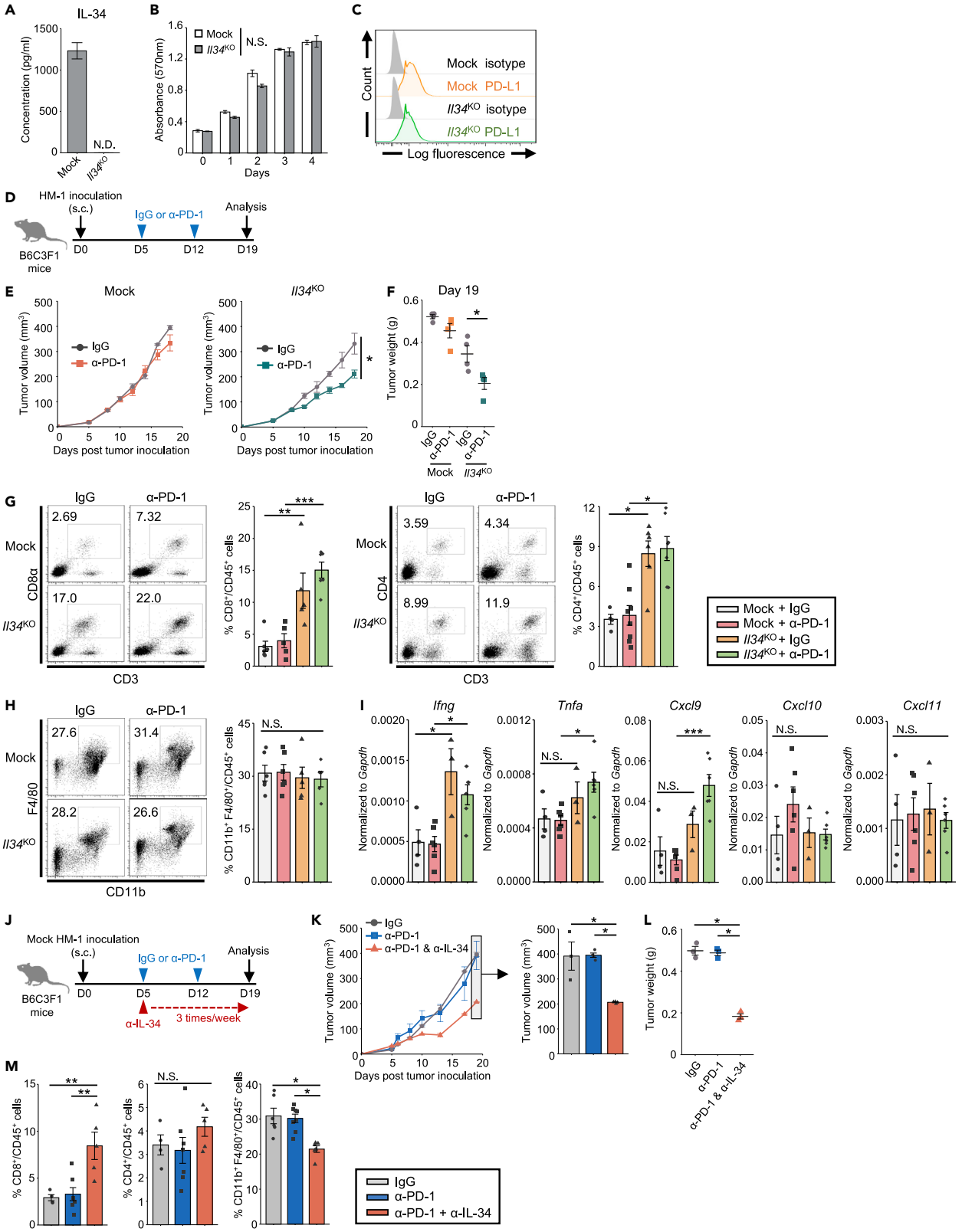
A
IL-34
Concentration (pg/ml)
1500
1000
500
0
N.D.
Mock
Il34KO
B
Mock
Il34KO
N.S.
Absorbance (570nm)
1.6
1.2
0.8
0.4
0
0 1 2 3 4
Days
C
Count
Mock isotype
Mock PD-L1
Il34KO isotype
Il34KO PD-L1
Log fluorescence
D
HM-1 inoculation
(s.c.)
IgG or α-PD-1
Analysis
B6C3F1
mice
D0 D5 D12 D19
E
Mock
Il34KO
Tumor volume (mm3)
IgG
α-PD-1
Days post tumor inoculation
F
Day 19
Tumor weight (g)
IgG
α-PD-1
Mock
Il34KO
G
IgG
α-PD-1
Mock
Il34KO
CD8α
CD3
2.69
7.32
17.0
22.0
% CD8+/CD45+ cells
3.59
4.34
8.99
11.9
CD4
% CD4+/CD45+ cells
Mock + IgG
Mock + α-PD-1
Il34KO + IgG
Il34KO + α-PD-1
H
F4/80
CD11b
27.6
31.4
28.2
26.6
% CD11b+ F4/80+/CD45+ cells
N.S.
I
Ifng
Tnfa
Cxcl9
Cxcl10
Cxcl11
Normalized to Gapdh
J
Mock HM-1 inoculation
(s.c.)
IgG or α-PD-1
Analysis
B6C3F1
mice
D0 D5 D12 D19
α-IL-34
3 times/week
K
IgG
α-PD-1
α-PD-1 & α-IL-34
Tumor volume (mm3)
Days post tumor inoculation
L
Tumor weight (g)
IgG
α-PD-1
α-PD-1 & α-IL-34
M
% CD8+/CD45+ cells
% CD4+/CD45+ cells
% CD11b+ F4/80+/CD45+ cells
IgG
α-PD-1
α-PD-1 + α-IL-34

Figure 1. IL-34 Derived from HM-1 Cells Limits Therapeutic Efficacy of Anti-PD-1. Therapy with Inhibiting T Cell Accumulation

(A) IL-34 concentration in supernatants of HM-1 cell lines (n = 3/cell line).

(B) Mean cell viability of Mock and Il34KO HM-1 cells measured by MTT assay (n = 3, technical triplicates). Similar results were obtained in 2 independent experiments.

(C) Representative histograms of PD-L1 expression of HM-1 cell lines.

(D) Schematic of the anti-PD-1 treatment. The timeline shows the procedure of tumor inoculation and antibody treatment.

(E) Tumor growth in B6C3F1 mice inoculated with Mock or Il34KO HM-1 cells and treated with anti-PD-1 antibody (α-PD-1) or control IgG (n = 4–6/group). Similar results were obtained in 2 independent experiments.

(F) Tumor weight on day 19 after tumor inoculation (n = 4/group).

(G) Representative flow cytometry profiles showing CD8+ and CD4+ T cells within the tumor-infiltrating CD3+CD45 + cells on day 19. Bar graphs represent the frequency of each T cell subset (n = 4–6/group).

(H) Representative flow cytometry profiles showing CD11b+ and F4/80 + cells within the tumor-infiltrating CD45 + cells on day 19. Bar graphs represent the frequency of CD11b + F4/80 + cells within CD45 + cells (n = 4–6/group).

(I) qPCR analysis of Ifng, Tnfa, Cxcl9, Cxcl10, and Cxcl11 mRNA expression in HM-1 tumors on day 19 (n = 3–6/group).

(J) Schematic of the anti-PD-1 antibody (α-PD-1) treatment in combination with anti-IL-34 antibody (α-IL-34). The timeline shows the procedure of tumor inoculation and antibody treatment.

(K) Mock HM-1 tumor growth in B6C3F1 mice treated with the indicated antibodies (n = 3–4/group). Similar results were obtained in 2 independent experiments.

(L) Tumor weight on day 19 after tumor inoculation (n = 4/group).

(M) Bar graphs represent the frequency of CD8+ or CD4+ cells within the CD3+CD45 + cells and CD11b + F4/80 + cells within CD45 + cells infiltrated in the tumors described in Figure 2B (n = 3–7/group).

Data represent mean ± SEM. *p < 0.05, **p < 0.01, ***p < 0.001; two-tailed Student's t-test (E), Tukey's multiple comparison test (F-M). N.S., not significant. See also Figures S1–S3.

IL-34 in the brain and skin, in contrast to CSF-1 which is widely expressed in the body under physiological conditions (Wang et al., 2012). However, despite its selective expression, IL-34 can be expressed and secreted by tumor cells and plays important roles in tumor progression (Baghdadi et al., 2018, 2019; Franzè et al., 2017; Lin et al., 2008; Ségaliny et al., 2015; Wang et al., 2012; Zhou et al., 2016) and resistance against chemotherapy and molecular targeted therapy (Baghdadi et al., 2016; Giricz et al., 2018). Except for our previous report of the potential involvement of IL-34 in tumor resistance against PD-1 blockade in a clinical case of a refractory melanoma patient (Han et al., 2018), little is known regarding the real role of IL-34 in promoting immunotherapeutic resistance against ICB and the related mechanisms. In this study, we first explore the potential role of IL-34 in mediating immune resistance of tumors against ICB in various murine tumors in addition to patient-derived xenograft (PDX) model and examine its impact on the molecular and cellular components of the TME.

RESULTS

IL-34-Expressing HM-1 Murine Ovarian Cancer Is Resistant to PD-1 Blockade Therapy

To evaluate the impact of IL-34 on the therapeutic effects of ICB, we first utilized a murine ovarian cancer cell line OV2944-HM-1 (HM-1), which secretes a substantial level of IL-34 (Figure 1A) and CSF-1 (Figure S1). We used CRISPR-Cas9 system to generate IL-34-deficient HM-1 cell line (named *Il34*^{KO} HM-1), and knockout efficiency was confirmed by measuring the secreted levels of IL-34 by Enzyme-Linked Immunosorbent Assay (ELISA) (Figure 1A). We found that the defect of IL-34 expression did not affect the viability of HM-1 cells *in vitro*, as compared with mock-transfected (Mock) HM-1 cells (Figure 1B). These cell lines expressed comparably low level of surface PD-L1 molecule (Figure 1C), while other surface molecules, including CD115 (CSF-1R), CD80, CD86, and PD-L2, were undetectable (data not shown). Then, Mock or *Il34*^{KO} HM-1 cells were subcutaneously (s.c.) injected into syngenic B6C3F1 mice to evaluate their response against PD-1 blockade (Figure 1D). Interestingly, only *Il34*^{KO} HM-1 tumors responded to PD-1 blockade, showing smaller tumor volumes than control IgG treatment (Figures 1E and 1F). On the other hand, PD-1 blockade showed little effects in mice bearing Mock HM-1 tumors (Figures 1E and 1F), indicating that PD-1 blockade is obvious in the absence of IL-34 in this model.

We then collected tumors on day 19 and subjected them to flow cytometry analysis. Interestingly, we found that *Il34*^{KO} HM-1 tumors were characterized by high infiltration of CD8^{+} and CD4^{+} T cells in the control IgG treatment group compared to Mock HM-1 tumors (Figure 1G), yet the enhancement of T cell infiltration in *Il34*^{KO} HM-1 tumors was independent of PD-1 blockade. Additionally, we found that the frequencies of CD11b^{+}F4/80^{+} cells were comparable among all groups and not affected by either IL-34 deficiency or PD-1 blockade (Figure 1H). Besides, quantitative PCR (qPCR) analysis showed enhanced expression of *Ifng* and *Tnfa* in *Il34*^{KO} HM-1 tumors (Figure 1I). Together, these data suggest that IL-34 secreted by tumor

cells, in itself, may disturb T cell-mediated antitumor immunity without affecting macrophage population, which apparently affected the efficacy of PD-1 blockade therapy.

The results shown above suggested that IL-34 derived from tumor cells controls T cell infiltration to tumor sites. Therefore, we sought to determine the factor that contributes to the chemotaxis of T cells. Cxcl9, Cxcl10, and Cxcl11 are known as T cell chemoattractants, and their expression is induced by IFNγ (Tokunaga et al., 2018). qPCR analysis revealed that, among these chemokines, *Cxcl9*, but not *Cxcl10* and *Cxcl11*, expression was significantly upregulated in the anti-PD-1 treated *Il34*^{KO} HM-1 tumors (Figure 1I). Cxcl9 has been shown to strongly stimulate T cell killer activity by binding to its receptor Cxcr3 (Chow et al., 2019), which may explain why the efficacy of PD-1 blockade was enhanced in *Il34*^{KO} HM-1 tumors. Additionally, we performed flow cytometry analysis to identify the cell types expressing CSF-1R (CD115) and the populations of these cells. As a result, we revealed that CD115^{+} cell subset consisted of several immune cells, CD11c^{+}MHC classII^{+}, CD11b^{+}F4/80^{+}, CD3ε^{+} cells, and others. Interestingly, these cell proportions were not affected by IL-34 knockout in HM-1, but the CD115^{+} cells population within tumor-infiltrating CD45^{+} cells was expanded (Figure S2). Our results suggested that tumor-derived IL-34 could suppress the differentiation, proliferation, or infiltration of CD115^{+} cells in TME.

Therapeutic Benefits of IL-34 Blockade with Neutralizing Antibody when Combined with anti-PD-1 Antibody *In Vivo*

Based on the above results, we aimed to evaluate the therapeutic benefits of IL-34 blockade when combined with immunotherapy. B6C3F1 mice were inoculated with Mock HM-1 cells (IL-34-expressing) and then treated with anti-PD-1 antibody alone or combined with IL-34-neutralizing antibody or control IgG (Figure 1J). Fourteen days after the onset of treatment, PD-1 blockade alone showed minimal effects on tumor size compared to the control group (Figures 1K and 1L). On the other hand, the combination of PD-1 blockade with anti-IL-34 antibody resulted in a significant suppression of tumor growth and tumor weight compared to anti-PD-1 monotherapy (Figures 1K and 1L). By analyzing the cellular components of the TME in each group, we found that IL-34 blockade resulted in enhanced infiltration of CD8^{+} T cells, but not CD4^{+} T cells (Figure 1M). In this case, in contrast to IL-34 knockout model, the frequency of CD11b^{+}F4/80^{+} cells showed a slight reduction in combination therapy (Figure 1M). This observation may be explained by broad effect of neutralizing antibody which targets IL-34 produced not only by tumor cells but also by other cell types within TME. Previous studies demonstrated that CSF-1R blockade enhances antitumor response through anti-PD-1 treatment in several cancer models. To compare the antitumor efficacy of IL-34 blockade with CSF-1R blockade, we next performed *in vivo* experiments using anti-CSF-1R antibody under the same protocol used in anti-IL-34 antibody treatment. As a result, similar to anti-IL-34 mAb treatment, the anti-CSF-1R treatment showed a decrease in tumor growth when combined with anti-PD-1 mAb treatment (Figure S3). These data indicate that IL-34 blockade has the potential to enhance the efficacy of anti-PD-1 mAb as well as CSF-1R blockade.

IL-34 Impairs the Therapeutic Effects of PD-1 Blockade in Murine Colon and Breast Cancer Models

To extend our findings on the immunosuppressive role of tumor cell-derived IL-34 against PD-1 blockade, we utilized two more murine cancer cell lines: CT26 colon cancer that shows low-level expression of IL-34, and 4T1 breast cancer that secretes considerable level of IL-34 (Figure 2A). CRISPR-Cas9 system was used to generate CT26 and 4T1 cell lines deficient in IL-34; in addition, expression of IL-34 was enforced in *Il34*^{KO} CT26 cell line to generate IL-34 overexpression cell line (*Il34*^{OE} CT26). We note that, similar to HM-1 cells, these cell lines also secreted CSF-1 (Figure S1). Syngenic BALB/c mice were inoculated with these tumor cells and treated with anti-PD-1 antibody or control IgG (Figures 2B and 2K). As expected, *Il34*^{KO} tumors exhibited a better response when treated with anti-PD-1 antibody, showing smaller tumor volumes than control IgG treatment, whereas the significant effect of PD-1 blockade was abrogated by the existence of IL-34 secreted by tumor cells (Figures 2C and 2L). To evaluate the gene set enhanced in the group showing the most effective antitumor efficacy, we performed next-generation sequencing (NGS) analysis and gene ontology (GO) analysis. The analyzed data suggested that the clusters associated with immune cell response, including "T cell receptor signaling pathway," "antigen processing and presentation," and "cytokine-cytokine receptor interaction," were enriched in the group inoculated with *Il34*^{KO} CT26 and treated with anti-PD-1 antibody (Figure S4). Moreover, we found that several genes associated with T cell accumulation (*Cd3e*, *Cd4*, *Cd8a*), inflammation (*Tnf*, *Ifng*, *Cxcl9*), and M1-macrophage subset (*Cd86*, *Ciita*, *Nos2*) were upregulated in *Il34*^{KO} CT26 tumor treated with anti-PD-1 antibody (Figure 2D).

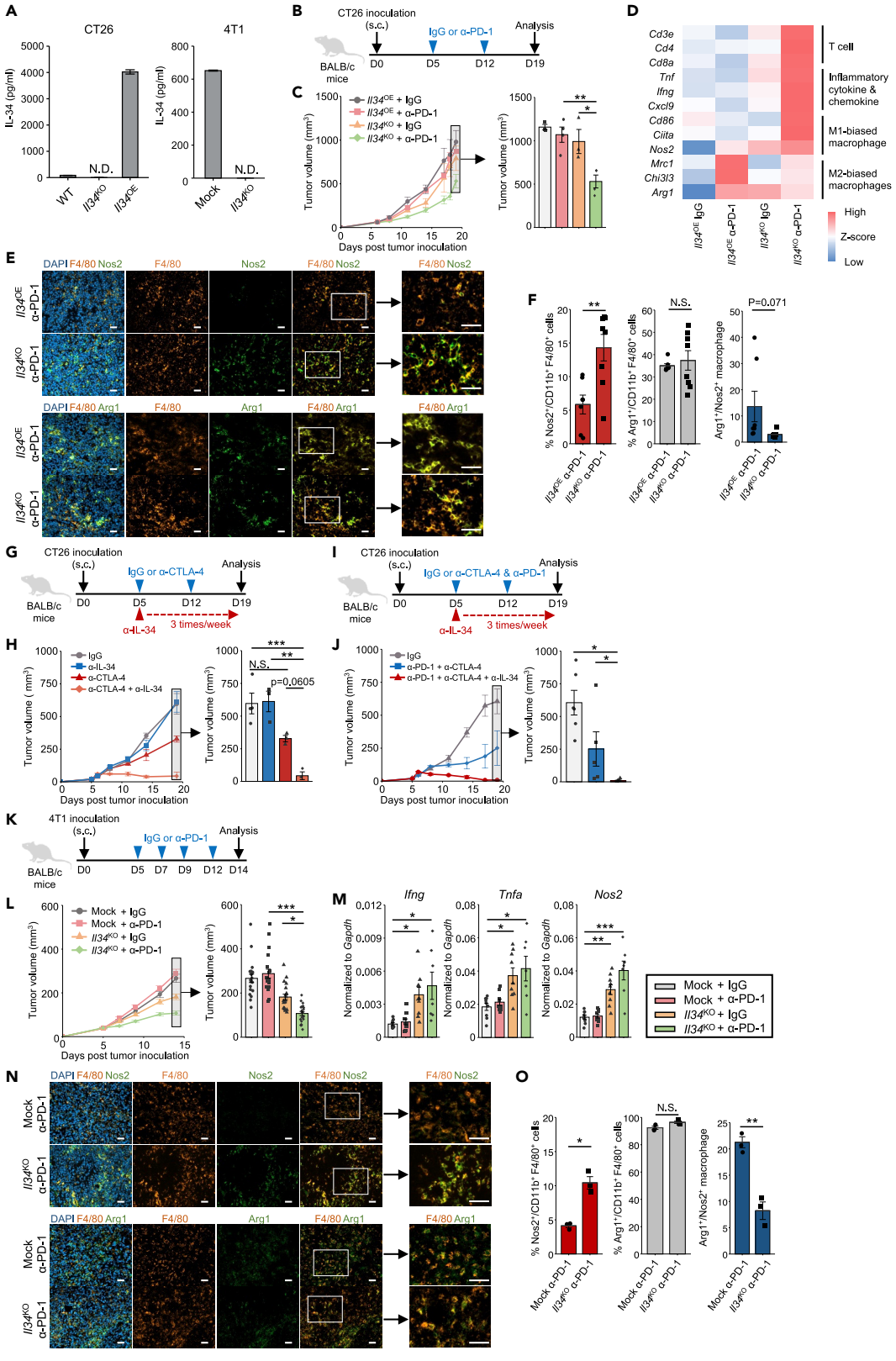
A
CT26
4T1
IL-34 (pg/ml)
N.D.
WT
Il34KO
Il34OE
Mock
B
CT26 inoculation
(s.c.)
IgG or α-PD-1
Analysis
BALB/c mice
D0
D5
D12
D19
C
Il34OE + IgG
Il34OE + α-PD-1
Il34KO + IgG
Il34KO + α-PD-1
Tumor volume (mm3)
Days post tumor inoculation
D
Cd3e
Cd4
Cd8a
Tnf
Ifng
Cxcl9
Cd86
Ciita
Nos2
Mrc1
Chi3l3
Arg1
T cell
Inflammatory cytokine & chemokine
M1-biased macrophage
M2-biased macrophages
High
Z-score
Low
E
DAPI F4/80 Nos2
F4/80
Nos2
DAPI F4/80 Arg1
Arg1
F
% Nos2+/CD11b+ F4/80+ cells
% Arg1+/CD11b+ F4/80+ cells
Arg1+/Nos2+ macrophage
N.S.
P=0.071
G
CT26 inoculation
(s.c.)
IgG or α-CTLA-4
Analysis
α-IL-34
3 times/week
I
IgG or α-CTLA-4 & α-PD-1
H
IgG
α-IL-34
α-CTLA-4
α-CTLA-4 + α-IL-34
p=0.0605
J
α-PD-1 + α-CTLA-4
α-PD-1 + α-CTLA-4 + α-IL-34
K
4T1 inoculation
(s.c.)
D0
D5
D7
D9
D12
D14
L
Mock + IgG
Mock + α-PD-1
Il34KO + IgG
Il34KO + α-PD-1
M
Ifng
Tnfa
Nos2
Normalized to Gapdh
N
O

Figure 2. Reversible Resistance against ICB of CT26 Colon Cancer and 4T1 Breast Cancer Cells by IL-34 Expression and Blockade

(A) IL-34 concentration in supernatants of WT, Il34KO, or Il34OE CT26 cells (n = 2/cell line, technical replicates) and Mock or Il34KO 4T1 cells (n = 2/cell line, technical replicates).

(B) Schematic of the anti-PD-1 antibody (α-PD-1) or control IgG treatment. The timeline shows the procedure of tumor inoculation and antibody treatment.

(C) Tumor growth in BALB/c mice inoculated with Il34KO or Il34OE CT26 cells and treated with anti-PD-1 antibody or control IgG (n = 3–4/group). Similar results were obtained in 2 independent experiments.

(D) Expression of selected genes is displayed by heatmap rendering of z-scores. Each column is the expression profile of a single tumor, and each row is a target gene, denoted on the left.

(E) Representative immunofluorescent stainings of F4/80, Nos2, and Arg1 of CT26 tumors. Green color indicates the expression of Nos2 (upper panel) or Arg1 (lower. panel) with F4/80 + macrophage infiltrating into tumor sites. Scale bars represent 20 μm.

(F) Proportions of Nos2+ or Arg1+ cells within the CT26 tumor-infiltrating CD11b + F4/80 + cells analyzed by flow cytometry on day 19. Bar graphs represent the frequency of each cell subset and the ratio of Arg1+ macrophage/Nos2+ macrophage (n = 8/group).

(G) Schematic of the anti-CTLA-4 or IL-34 antibody (α-CTLA-4, α-IL-34) or control IgG treatment. The timeline shows the procedure of tumor inoculation and antibody treatment.

(H) Tumor growth in BALB/c mice inoculated with Il34OE CT26 cells and treated with anti-CTLA-4 and/or IL-34 antibodies or control IgG (n = 3–4/group). Similar results were obtained in 2 independent experiments.

(I) Schematic of the anti-PD-1, CTLA-4 or IL-34 antibody, or control IgG treatment. The timeline shows the procedure of tumor inoculation and antibody treatment.

(J) Tumor growth in BALB/c mice inoculated with Il34OE CT26 cells and treated with anti-PD-1 and CTLA-4 antibodies with or without IL-34 antibody or control IgG (n = 5-7/group). Similar results were obtained in 2 independent experiments.

(K) Schematic of the anti-PD-1 antibody (α-PD-1) or control IgG treatment. The timeline shows the procedure of tumor inoculation and antibody treatment.

(L) Tumor growth in BALB/c mice inoculated with Mock or Il34KO 4T1 cells and treated with anti-PD-1 antibody or control IgG (n = 20/group). Similar results were obtained in 6 individual experiments.

(M) qPCR analysis of Ifng, Tnfa, and Nos2 mRNA expression in tumors on day 14 described in Figure 2J (n = 7/group).

(N) Representative immunofluorescent stainings of F4/80, Nos2, and Arg1 of 4T1 tumors. Green color indicates the expression of Nos2 (upper) or Arg1 (down) with F4/80 + macrophage infiltrating into tumor sites. Scale bars represent 20 μm.

(O) Proportions of Nos2+ or Arg1+ cells within the 4T1 tumor-infiltrating CD11b + F4/80 + cells analyzed by flow cytometry on day 14. Bar graphs represent the frequency of each cell subset and the ratio of Arg1+ macrophage/Nos2+ macrophage (n = 3/group).

Data represent mean ± SEM. *$p < 0.05$, **$p < 0.01$; Tukey's multiple comparison test (C, K, L) or Steel-Dwass nonparametric multiple comparison test (G, I), Student's t-test (E.M). N.S., not significant.

See also Figures S1, S4, and S5.

On the other hand, gene expressions of M2-macrophage subset (*Mrc1*, *Chi3l3*, *Arg1*) in $Il34^{KO}$ CT26 tumor was lower than in $Il34^{OE}$ CT26 tumor treated with anti-PD-1 antibody (Figure 2D). We also performed qPCR to evaluate the expression of several genes presented in Figure 2D using CT26 and 4T1 tumor samples (Figure S5).

Next, we performed immunofluorescence staining and flow cytometry analysis to demonstrate whether tumor-derived IL-34 contributes to the populations of M1- and M2-biased macrophage in TME. As a result, the tumor-infiltrating $Nos2^{+}$ M1-biased macrophage population was upregulated, and the ratio of $Arg1^{+}$ M2-biased macrophage to $Nos2^{+}$ M1-biased macrophage was decreased in $Il34^{KO}$ CT26 tumor (Figures 2E and 2F). These data suggest that tumor-derived IL-34 can interfere with the expansion of M1-biased macrophage in TME and form an anti-inflammatory microenvironment. 4T1 tumors, as well as CT26 tumors, showed significantly higher expression of inflammatory and pro-inflammatory cytokines when treated with PD-1 inhibitor (Figure 2M). Also, the population of tumor-infiltrating M1-biased macrophage was increased in $Il34^{KO}$ 4T1 tumor (Figures 2N and O).

With the indent to additionally evaluate IL-34 relevance to ICB resistance, we treated $Il34^{OE}$ CT26 tumors with anti-CTLA-4 antibody in combination with anti-IL-34 antibody (Figure 2G). $Il34^{OE}$ CT26 tumors treated with anti-CTLA-4 antibody exhibited a trend toward growth suppression ($p = 0.06$), and one of the tumors was completely eliminated (Figure 2H). Next, we tested the combination therapy of anti-PD-1 and CTLA-4 antibodies to treat $Il34^{OE}$ CT26 tumors with or without anti-IL-34 antibody (Figure 2I). While PD-1 and CTLA-4 combination therapy showed substantial tumor suppression, additional anti-IL-34 treatment resulted in a dramatical suppression. Among this treatment group, 2 out of 5 tumors were completely rejected (Figure 2J).

Collectively, these data indicate that IL-34 limits the efficacy of ICB not only by interfering T cell accumulation but also by reforming TME into the anti-inflammatory environment through the increase of M1-macrophage population. Also, IL-34 inhibition therapy with a neutralizing antibody efficiently reverses ICB resistance through recovering inflammatory circuit in the TME.

Therapeutic Potential of IL-34 Blockade in a PDX Model of Human Lung Adenocarcinoma

Finally, to translate these findings into clinical settings, we utilized a PDX model in which humanized-NOD.Cg-*Prkdc*^{scid}*Il2rg*^{tm1Wjl}/SzJ (NSG) mice, pre-injected with human hematopoietic stem cells (HSC), named HuNSG, were transplanted with human primary lung adenocarcinoma tissues (for detailed information, refer to Methods section). The tumor tissues exhibited considerable expression of both IL-34 and PD-L1 (Figures 3A–3C). HuNSG mice with established tumors were then treated with a monotherapy of anti-PD-1 or IL-34 antibody or a combination of both antibodies (Figure 3D). As a result, PD-1 blockade alone showed poor response when compared to the control baseline (Figure 3E). Anti-IL-34 monotherapy suppressed tumor growth in 1 out of 3 tumors, while the combination of anti-PD-1 and anti-IL-34 antibodies resulted in substantially suppressed tumor growth in 2 out of 3 tumors (Figure 3E). We observed complete necrosis in 1 responded tumor of the combination therapy group, and therefore, the tumor cannot be collected and not proceeded to further analyses (Figure 3F), suggesting that the combination therapy unleashed strong antitumor effect. Consistent with these data, strong immune cell infiltration was observed in the responded tumor in the combination therapy group (Figure 3G).

Thus, these data suggest that IL-34 is involved in ICB resistance of human cancer and that its inhibition restores the therapeutic effect of ICB.

DISCUSSION

In this study, we identify for the first time a potential involvement of IL-34 in immunotherapeutic resistance of cancer. By targeting IL-34 in the murine HM-1 ovarian cancer cells and 4T1 breast cancer cells using CRISPR-Cas9 system, we found that IL-34-deficient tumors exhibit a better response to therapeutic ICB than IL-34-expressing tumors. Nevertheless, CT26 murine colon cancer cells are known to be responsive to immune checkpoint inhibitors including anti-PD-1 and anti-CTLA-4 antibodies (Fu et al., 2019; Jure-Kunkel et al., 2013), overexpression of IL-34 in the cell line significantly impaired the outcome of ICB. More importantly, a neutralizing antibody against IL-34 showed therapeutic potential when combined with PD-1 blockade, which was further confirmed in a PDX model of lung adenocarcinoma.

By analyzing the cellular components of the TME in our therapeutic models, we found that IL-34 converts not only the cellular profiles within tumor site but also the inflammatory state of TME. It is already reported that CSF-1R blockade induces a dramatical decline of the macrophage population in tumor sites (MacDonald et al., 2010). However, this phenomenon was not fully recapitulated in IL-34 blockade treatment that macrophage population showed only a slight reduction (Figure 1M). These results led us to the hypothesis that IL-34 may affect the function rather than the frequencies of tumor-infiltrating myeloid cells. Consistent with this, the existence of tumor-derived IL-34 suppressed the expression of *Cxcl9* responsible for T cell recruitment and activation (Figure 1I). Additionally, we found that the expression levels of inflammatory and pro-inflammatory factors such as *Ifng*, *Tnfa, and Nos2* were higher in IL-34-deficient tumors (Figures 1I. 2D, and M), which may support the hypothesis that IL-34 modifies the function of tumor-infiltrating myeloid cells at the local TME. In accordance with this, immunofluorescence staining revealed the possible role of IL-34 to restrict the M1 polarization of tumor-infiltrating macrophage (Figures 2E, F, N, and O).

Although IL-34 shows similar biological activities with CSF-1 *in vitro*, several studies have reported differences in the response of myeloid cells toward IL-34 or CSF-1 stimulation, showing altered expression of pro-inflammatory cytokines and chemokines (Boulakirba et al., 2018; Nakamichi et al., 2013). The engagement of CSF-1R by IL-34 has been suggested to activate caspase and autophagy signaling pathways in monocytes, which results in an IL-34-induced macrophagic differentiation and polarization that differ from CSF-1 (Boulakirba et al., 2018). Differences in CSF-1R binding affinity, hydrophobic/hydrophilic binding feature, in addition to differences in the binding pockets have been suggested to explain the distinct signaling between IL-34 and CSF-1 (Boulakirba et al., 2018; Liu et al., 2012). However, the molecular mechanisms that explain such differences remain to be explored in future works (Boulakirba et al., 2018).

Accumulating evidence has indicated critical roles for tumor-derived cytokines in all aspects of the TME, including tumor growth, metastasis, angiogenesis, and therapeutic resistance (Chen et al., 2018; Eichbaum et al., 2011; Jones et al., 2016; Kim et al., 2006). Accordingly, many cytokines may serve as beneficial therapeutic targets in cancer (Berraondo et al., 2019; Lee and Margolin, 2011; Rossi et al., 2015; Setrerrahmane and Xu, 2017; Szebeni et al., 2016). As an alternative ligand to CSF-1 for CSF-1R, IL-34 is suggested to play important roles at the TME by direct effects on both tumor and immune cells (Baghdadi et al.,

A

Model ID	Primary Site	PDX Pathology	Tumor Site	Tumor Type	IL-34 (FPKM)	PD-L1 (FPKM)
LU-TM-0007	Lung	Adenocarcinoma	Lung	Primary	13.575	29.841

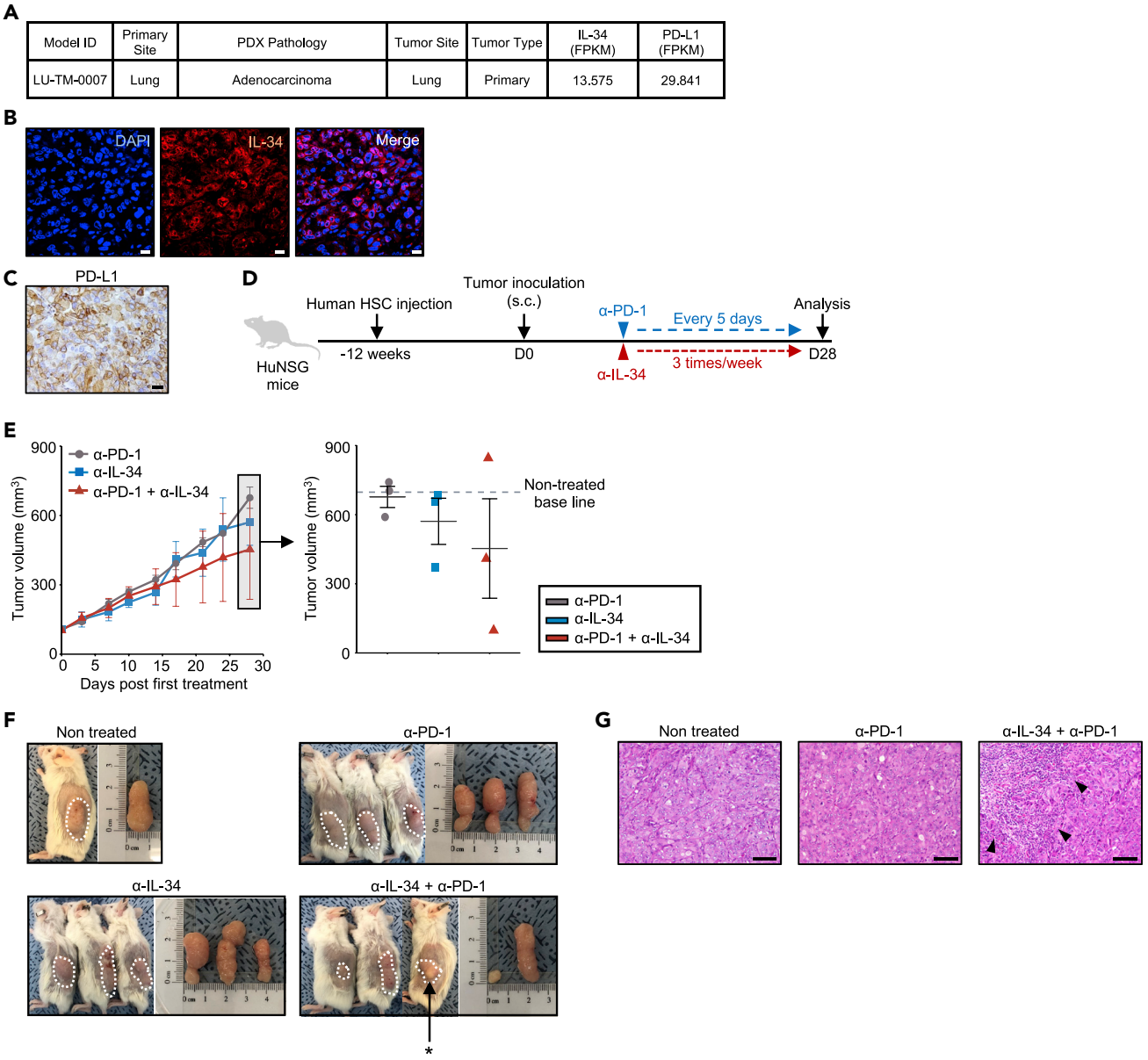

Figure 3. Anti-IL-34 Treatment Enhances the Efficacy of Anti-PD-1 Treatment in PDX Model

(A) Pathological and gene expression profile of the tumor tissue used for the establishment of PDX model.

(B) Immunofluorescence staining of LU-TM-0007 sample for IL-34. Nuclei were counterstained with DAPI. Scale bars represent 20 μm.

(C) Representative immunohistochemistry staining of LU-TM-0007 sample with PD-L1 in the tumor. Scale bar represents 20 μm.

(D) Schematic of the anti-PD-1 (α-PD-1) and/or IL-34 (α-IL-34) antibody treatment. The timeline shows the procedure of human HSC injection, tumor inoculation, and antibody treatment.

(E) Tumor growth in HuNSG mice inoculated with LU-TM-0007 tumor cells and treated with the antibodies (n = 3/group). Dotted line indicates the size of nontreated tumor at the same time point. Dot plot shows the tumor size on day 28. Individual data points are shown with mean ± SEM.

(F) Macroscopic observation of s.c. injected xenografts in HuNSG mice sacrificed on day 28. Combination therapy caused strong necrosis in one of the treated tumors (*) which could not be further analyzed.

(G) Representative hematoxylin and eosin staining of resected tumors in nontreated, anti-PD-1, or combination therapy groups on day 28. Arrowheads indicate infiltrating immune cells. Scale bars represent 100 μm.

2016). Thus, neutralizing antibodies that target IL-34 or specific inhibitors that suppress IL-34 expression may help to control tumor progression and overcome the resistance problem. In this study, all murine cancer cell lines, including the genetically manipulated ones, expressed CSF-1 simultaneously with IL-34

(Figures 1A and S1). Despite the fact that tumor-derived CSF-1 may be released in TME, IL-34 blockade enhanced the efficacy of immune checkpoint blockade *in vivo*. It indicates that IL-34-expressing tumors may acquire resistance to immune checkpoint blockade independently of CSF-1 existence. Possible merit of targeting IL-34 in cancer is the fewer side effects that result from treatment, due to the limited expression of IL-34 under physiological conditions. On the other hand, it has been reported that IL-34 binds to other receptors, protein tyrosine phosphatase, receptor type Z, polypeptide 1 (PTPRZ1), and Syndecan-1. PTPRZ1 is primarily expressed on neuronal progenitors and glial cells. Via PTPRZ1, IL-34 can regulate intracellular signaling pathways that inhibit proliferation, clonogenicity, and motility of the cellular targets, indicating a CSF1-R-independent action (Nandi et al., 2013). Syndecan-1 is involved in cell proliferation, migration, and matrix interactions, expressed in a wide range of tissues. Syndecan-1 and IL-34 binding modulates IL-34-induced CSF-1R activation and affects a particular myeloid cell migration (Ségaliny et al., 2015). Altogether, it is possible that IL-34 exerts its biological activities through binding to PTPRZ1 and syndecan-1 in addition to interaction with CSF-1R in TME. However, whether blocking IL-34 binding to these receptors interferes with antitumor effect or causes adverse effects remains unclear. This is also supported by the phenotype of *Il34* knockout mice that showed no remarkable effects in contrast to *Csf1r* or *Csf1* knockout mice (Wang et al., 2012). Furthermore, our finding in this study that IL-34 blockade does not severely decrease the frequency but enhance the function of myeloid cells may be a great advance compared with the total CSF-1R blockade in which myeloid cell population is dramatically destroyed (MacDonald et al., 2010).

In conclusion, we added here new evidence that indicates a potential role for IL-34 in promoting therapeutic resistance against tumor immunotherapy. These results indicate that IL-34 could be a therapeutic target to enhance the efficacy of ICB in human cancer treatment.

Limitations of the Study

Here, we demonstrated tumor-derived IL-34 has potential as a target for therapy that enhances the efficacy of ICB, regardless of the expression of CSF-1 from tumor cells. However, the molecular mechanism that explains the difference between IL-34 and CSF-1 on the immune system in TME needs to be elucidated in further research.

Resource Availability

Lead Contact

Ken-ichiro Seino, Division of Immunobiology, Institute for Genetic Medicine, Hokkaido University, Kita-15 Nishi-7, Sapporo 060-0815, Japan (seino@igm.hokudai.ac.jp).

Materials Availability

Not applicable.

Data and Code Availability

The NGS data in this paper have been deposited in GEO repository (https://www.ncbi.nlm.nih.gov/geo/query/acc.cgi?acc=GSE157602).

METHODS

All methods can be found in the accompanying Transparent Methods supplemental file.

SUPPLEMENTAL INFORMATION

Supplemental information can be found online at https://doi.org/10.1016/j.isci.2020.101584.

ACKNOWLEDGMENTS

The authors thank Ms. Yui Umeyama for her helpful technical supports. This work was supported in part by the Japan Agency for Medical Research and Development (AMED; Practical Research for Innovative Cancer Control) (K.-S.).

AUTHOR CONTRIBUTION

MB and KS designed the study. Naoki H, TK, Nanumi H, FK, NK, HW, HY, HL, and HR performed experiments. All authors analyzed data and discussed the results. Naoki H, TK, Nanumi H, RO, MB, and KS contributed to manuscript preparation. All authors approved the final version of this manuscript.

DECLARATION OF INTERESTS

The authors disclosed no potential conflicts of interest.

Received: February 24, 2020
Revised: August 4, 2020
Accepted: September 16, 2020
Published: October 23, 2020

REFERENCES

Baghdadi, M., Wada, H., Nakanishi, S., Abe, H., Han, N., Wira, E.P., Endo, D., Watari, H., Sakuragi, N., Hida, Y., et al. (2016). Chemotherapy-induced IL34 enhances immunosuppression by tumor-associated macrophages and mediates survival of chemoresistant lung cancer cells. Cancer Res. *76*, 6030–6042.

Baghdadi, M., Endo, H., Takano, A., Ishikawa, K., Kameda, Y., Wada, H., Miyagi, Y., Yokose, T., Ito, H., Nakayama, H., et al. (2018). High co-expression of IL-34 and M-CSF correlates with tumor progression and poor survival in lung cancers. Sci. Rep. *8*, 1–10.

Baghdadi, M., Ishikawa, K., Nakanishi, S., Murata, T., Umeyama, Y., Kobayashi, T., Kameda, Y., Endo, H., Wada, H., Bogen, B., et al. (2019). A role for IL-34 in osteolytic disease of multiple myeloma. Blood Adv. *3*, 541–551.

Berraondo, P., Sanmamed, M.F., Ochoa, M.C., Etxeberria, I., Aznar, M.A., Pérez-Gracia, J.L., Rodríguez-Ruiz, M.E., Ponz-Sarvise, M., Castañón, E., and Melero, I. (2019). Cytokines in clinical cancer immunotherapy. Br. J. Cancer *120*, 6–15.

Binnewies, M., Roberts, E.W., Kersten, K., Chan, V., Fearon, D.F., Merad, M., Coussens, L.M., Gabrilovich, D.I., Ostrand-Rosenberg, S., Hedrick, C.C., et al. (2018). Understanding the tumor immune microenvironment (TIME) for effective therapy. Nat. Med. *24*, 541–550.

Boulakirba, S., Pfeifer, A., Mhaidly, R., Obba, S., Goulard, M., Schmitt, T., Chaintreuil, P., Calleja, A., Furstoss, N., Orange, F., et al. (2018). IL-34 and CSF-1 display an equivalent macrophage differentiation ability but a different polarization potential. Sci. Rep. *8*, 1–11.

Cannarile, M.A., Weisser, M., Jacob, W., Jegg, A.M., Ries, C.H., and Rüttinger, D. (2017). Colony-stimulating factor 1 receptor (CSF1R) inhibitors in cancer therapy. J. Immunother. Cancer *5*, 1–13.

Chen, Y., Tan, W., and Wang, C. (2018). Tumor-associated macrophage-derived cytokines enhance cancer stem-like characteristics through epithelial–mesenchymal transition. Onco. Targets Ther. *11*, 3817–3826.

Cheng, W., Fu, D., Xu, F., and Zhang, Z. (2018). Unwrapping the genomic characteristics of urothelial bladder cancer and successes with immune checkpoint blockade therapy. Oncogenesis *7*, 2.

Chow, M.T., Ozga, A.J., Servis, R.L., Frederick, D.T., Lo, J.A., Fisher, D.E., Freeman, G.J., Boland, G.M., and Luster, A.D. (2019). Intratumoral activity of the CXCR3 chemokine system is required for the efficacy of anti-PD-1 therapy. Immunity *50*, 1498–1512.e5.

Eichbaum, C., Meyer, A.S., Wang, N., Bischofs, E., Steinborn, A., Bruckner, T., Brodt, P., Sohn, C., and Eichbaum, M.H.R. (2011). Breast cancer cell-derived cytokines, macrophages and cell adhesion: implications for metastasis. Anticancer Res. *31*, 3219–3227.

Franzè, E., De Simone, V., Dinallo, V., Rizzo, A.M., Caprioli, F., Colantoni, A., Ortenzi, A., Sica, G., and Monteleone, G. (2017). OC.01.4: interleukin-34 sustains pro-tumorigenic signals in colon cancer tissue. Dig. Liver Dis. *49*, e78.

Fu, C., Zhu, X., Xu, P., and Li, Y. (2019). Pharmacological inhibition of USP7 promotes antitumor immunity and contributes to colon cancer therapy. Onco. Targets Ther. *12*, 609–617.

Garon, E.B., Rizvi, N.A., Hui, R., Leighl, N., Balmanoukian, A.S., Eder, J.P., Patnaik, A., Aggarwal, C., Gubens, M., Horn, L., et al. (2015). Pembrolizumab for the treatment of non–small-cell lung cancer. N. Engl. J. Med. *372*, 2018–2028.

Ghirelli, C., and Hagemann, T. (2013). Targeting immunosuppression for cancer therapy. J. Clin. Invest. *123*, 2355–2357.

Giricz, O., Mo, Y., Dahlman, K.B., Cotto-Rios, X.M., Vardabasso, C., Nguyen, H., Matusow, B., Bartenstein, M., Polishchuk, V., Johnson, D.B., et al. (2018). The RUNX1/IL-34/CSF-1R axis is an autocrinally regulated modulator of resistance to BRAF-V600E inhibition in melanoma. JCI Insight *3*, e120422.

Gyori, D., Lim, E.L., Grant, F.M., Spensberger, D., Roychoudhuri, R., Shuttleworth, S.J., Okkenhaug, K., Stephens, L.R., and Hawkins, P.T. (2018). Compensation between CSF1R+ macrophages and Foxp3+ Treg cells drives resistance to tumor immunotherapy. JCI Insight *3*, e120631.

Han, N., Baghdadi, M., Ishikawa, K., Endo, H., Kobayashi, T., Wada, H., Imafuku, K., Hata, H., and Seino, K. (2018). Enhanced IL-34 expression in Nivolumab-resistant metastatic melanoma. Inflamm. Regen. *38*, 2–6.

Herbst, R.S., Soria, J.C., Kowanetz, M., Fine, G.D., Hamid, O., Gordon, M.S., Sosman, J.A., McDermott, D.F., Powderly, J.D., Gettinger, S.N., et al. (2014). Predictive correlates of response to the anti-PD-L1 antibody MPDL3280A in cancer patients. Nature *515*, 563–567.

Hodi, F.S., O'Day, S.J., McDermott, D.F., Weber, R.W., Sosman, J.A., Haanen, J.B., Gonzalez, R., Robert, C., Schadendorf, D., Hassel, J.C., et al. (2010). Improved survival with ipilimumab in patients with metastatic melanoma. N. Engl. J. Med. *363*, 711–723.

Hugo, W., Zaretsky, J.M., Sun, L., Song, C., Moreno, B.H., Hu-Lieskovan, S., Berent-Maoz, B., Pang, J., Chmielowski, B., Cherry, G., et al. (2016). Genomic and transcriptomic features of response to anti-PD-1 therapy in metastatic melanoma. Cell *165*, 35–44.

Jones, V.S., Huang, R.Y., Chen, L.P., Chen, Z.S., Fu, L., and Huang, R.P. (2016). Cytokines in cancer drug resistance: cues to new therapeutic strategies. Biochim. Biophys. Acta *1865*, 255–265.

Jure-Kunkel, M., Masters, G., Girit, E., Dito, G., Lee, F., Hunt, J.T., and Humphrey, R. (2013). Synergy between chemotherapeutic agents and CTLA-4 blockade in preclinical tumor models. Cancer Immunol. Immunother. *62*, 1533–1545.

Kim, R., Emi, M., Tanabe, K., and Arihiro, K. (2006). Tumor-driven evolution of immunosuppressive networks during malignant progression. Cancer Res. *66*, 5527–5536.

Kumar, V., Patel, S., Tcyganov, E., and Gabrilovich, D.I. (2016). The nature of myeloid-derived suppressor cells in the tumor microenvironment. Trends Immunol. *37*, 208–220.

Lee, S., and Margolin, K. (2011). Cytokines in cancer immunotherapy. Cancers (Basel) *3*, 3856–3893.

Lin, H., Lee, E., Hestir, K., Leo, C., Huang, M., Bosch, E., Halenbeck, R., Wu, G., Zhou, A., Behrens, D., et al. (2008). Discovery of a cytokine and its receptor by functional screening of the extracellular proteome. Science *320*, 807–811.

Liu, H., Leo, C., Chen, X., Wong, B.R., Williams, L.T., Lin, H., and He, X. (2012). The mechanism of

shared but distinct CSF-1R signaling by the non-homologous cytokines IL-34 and CSF-1. Biochim. Biophys. Acta *1824*, 938–945.

MacDonald, K.P.A., Olver, S., Raffelt, N.C., Kuns, R., Hill, G.R., Palmer, J.S., Cronau, S., Seppanen, E., Wainwright, B., Pettit, A.R., et al. (2010). An antibody against the colony-stimulating factor 1 receptor depletes the resident subset of monocytes and tissue- and tumor-associated macrophages but does not inhibit inflammation. Blood *116*, 3955–3963.

Nakamichi, Y., Udagawa, N., and Takahashi, N. (2013). IL-34 and CSF-1: similarities and differences. J. Bone Miner. Metab. *31*, 486–495.

Nandi, S., Ciose, M., Yeung, Y.G., Nieves, E., Tesfa, L., Lin, H., Hsu, A.W., Halenbeck, R., Cheng, H.Y., Gokhan, S., et al. (2013). Receptor-type protein-tyrosine phosphatase ζ is a functional receptor for interleukin-34. J. Biol. Chem. *288*, 21972–21986.

Neubert, N.J., Bordry, N., Wald, N., Martignier, C., Tillé, L., Homicsko, K., Maby-El Hajjami, H., Ioannidou, K., Coukos, G., Fuertes Marraco, S.A., et al. (2018). T cell-induced CSF1 promotes melanoma resistance to PD1 blockade. Sci. Transl. Med. *10*, eaan3311.

Noy, R., and Pollard, J.W. (2014). Tumor-associated macrophages: from mechanisms to therapy. Immunity *41*, 49–61.

O'Donnell, J.S., Long, G.V., Scolyer, R.A., Teng, M.W.L., and Smyth, M.J. (2017). Resistance to PD1/PDL1 checkpoint inhibition. Cancer Treat. Rev. *52*, 71–81.

Pardoll, D.M. (2012). The blockade of immune checkpoints in cancer immunotherapy. Nat. Rev. Cancer *12*, 252–264.

Pitt, J.M., Marabelle, A., Eggermont, A., Soria, J.C., Kroemer, G., and Zitvogel, L. (2016). Targeting the tumor microenvironment: removing obstruction to anticancer immune responses and immunotherapy. Ann. Oncol. *27*, 1482–1492.

Prima, V., Kaliberova, L.N., Kaliberov, S., Curiel, D.T., and Kusmartsev, S. (2017). COX2/mPGES1/PGE2 pathway regulates PD-L1 expression in tumor-associated macrophages and myeloid-derived suppressor cells. Proc. Natl. Acad. Sci. U S A *114*, 1117–1122.

Quaranta, V., Rainer, C., Nielsen, S.R., Raymant, M.L., Ahmed, M.S., Engle, D.D., Taylor, A., Murray, T., Campbell, F., Palmer, D.H., et al. (2018). Macrophage-derived granulin drives resistance to immune checkpoint inhibition in metastatic pancreatic cancer. Cancer Res. *78*, 4253–4269.

Ribas, A. (2015). Adaptive immune resistance: how cancer protects from immune attack. Cancer Discov. *5*, 915–919.

Rossi, J.F., Lu, Z.Y., Jourdan, M., and Klein, B. (2015). Interleukin-6 as a therapeutic target. Clin. Cancer Res. *21*, 1248–1257.

Ségaliny, A.I., Mohamadi, A., Dizier, B., Lokajczyk, A., Brion, R., Lanel, R., Amiaud, J., Charrier, C., Boisson-Vidal, C., and Heymann, D. (2015). Interleukin-34 promotes tumor progression and metastatic process in osteosarcoma through induction of angiogenesis and macrophage recruitment. Int. J. Cancer *137*, 73–85.

Setrerrahmane, S., and Xu, H. (2017). Tumor-related interleukins: old validated targets for new anti-cancer drug development. Mol. Cancer *16*, 1–17.

Szebeni, G.J., Vizler, C., Nagy, L.I., Kitajka, K., and Puskas, L.G. (2016). Pro-tumoral inflammatory myeloid cells as emerging therapeutic targets. Int. J. Mol. Sci. *17*, 1958.

Tokunaga, R., Zhang, W., Naseem, M., Puccini, A., Berger, M.D., Soni, S., McSkane, M., Baba, H., and Lenz, H.J. (2018). CXCL9, CXCL10, CXCL11/CXCR3 axis for immune activation – a target for novel cancer therapy. Cancer Treat. Rev. *63*, 40–47.

Ugel, S., De Sanctis, F., Mandruzzato, S., and Bronte, V. (2015). Tumor-induced myeloid deviation: when myeloid-derived suppressor cells meet tumor-Associated macrophages. J. Clin. Invest. *125*, 3365–3376.

Wang, D.Y., Eroglu, Z., Ozgun, A., Leger, P.D., Zhao, S., Ye, F., Luke, J.J., Joseph, R.W., Haq, R., Ott, P.A., et al. (2017). Clinical features of acquired resistance to anti–PD-1 therapy in advanced melanoma. Cancer Immunol. Res. *5*, 357–362.

Wang, Y., Szretter, K.J., Vermi, W., Gilfillan, S., Rossini, C., Cella, M., Barrow, A.D., Diamond, M.S., and Colonna, M. (2012). IL-34 is a tissue-restricted ligand of CSF1R required for the development of Langerhans cells and microglia. Nat. Immunol. *13*, 753–760.

Zhou, S.L., Hu, Z.Q., Zhou, Z.J., Dai, Z., Wang, Z., Cao, Y., Fan, J., Huang, X.W., and Zhou, J. (2016). miR-28-5p-IL-34-macrophage feedback loop modulates hepatocellular carcinoma metastasis. Hepatology *63*, 1560–1575.

Zhu, Y., Yang, J., Xu, D., Gao, X.M., Zhang, Z., Hsu, J.L., Li, C.W., Lim, S.O., Sheng, Y.Y., Zhang, Y., et al. (2019). Disruption of tumour-associated macrophage trafficking by the osteopontin-induced colony-stimulating factor-1 signalling sensitises hepatocellular carcinoma to anti-PD-L1 blockade. Gut *68*, 1653–1666.

iScience, Volume *23*

Supplemental Information

Interleukin-34 Limits the Therapeutic Effects of Immune Checkpoint Blockade

Naoki Hama, Takuto Kobayashi, Nanumi Han, Fumihito Kitagawa, Nabeel Kajihara, Ryo Otsuka, Haruka Wada, Hee-kyung Lee, Hwanseok Rhee, Yoshinori Hasegawa, Hideo Yagita, Muhammad Baghdadi, and Ken-ichiro Seino

Transparent Methods

Cell lines

The ovarian cancer cell line OV2944-HM-1 (HM-1) was purchased from the Japanese Collection of Research Bioresources.The colon cancer cell line CT26 used in this study was kindly provided by Dr. Hidemitsu Kitamura, Hokkaido University. The breast cancer cell line 4T1 was purchased from American Type Culture Collection. HM-1 cell line was maintained in αMEM (Fujifilm Wako Pure Chemical Industries). CT26 and 4T1 cell lines were maintained in RPMI-1640 (Fujifilm Wako Pure Chemical Industries). All culture media were supplemented with 10% fetal bovine serum (Sigma Aldrich), 1% Penicillin/Streptomycin (Nacalai Tesque), and 1% Non-Essential Amino Acid (Nacalai Tesque). Cells were maintained in a 5% CO_2/air environment at 37℃.

Mice and *in vivo* assay

Six to eight-week-old female B6C3F1 and BALB/c mice were purchased from Japan SLC, Inc. The mice were maintained under specific pathogen-free conditions in the animal facility at Hokkaido University. For *in vivo* assay, 2×10^5 tumor cells were inoculated s.c. into the right flank of syngeneic female mice. Antibody treatment (anti-PD-1 (RMP1-14), 250 μg/mouse; CTLA-4 (UC10-4F10), 250 μg/mouse; or IL-34 (C054-35), 200 μg/mouse

was started when tumor size reached 5 mm in diameter. Anti-PD-1 and anti-CTLA-4 antibodies were kindly provided by Dr. Hideo Yagita (Juntendo University). Anti-IL-34 antibody was purchased from BioLegend. Detailed information about antibodies is described in Supplementary Table 1. All animal procedures were approved by the Hokkaido University Animal Care Committee (Approval number: 14-0171).

Generation of *Il34* knockout and *Il34* overexpression cell lines

Il34^{KO} cell line was generated by using IL-34 CRISPR/Cas9 KO Plasmid (m) (Santa Cruz Biotechnology, Inc.). The plasmids were transfected by using *Trans*IT-X2 (Mirus) or Neon® Transfection system (Thermo Fisher Scientific). Cells were selected by GFP expression 48 hours after transfection. For the generation of *Il34* overexpression CT26 cell line, mouse *Il34* coding sequence was cloned into pLenti-EF1a-C-Myc-DDK-IRES-Puro vector (Origene). Lenti-X293T cells were transfected with lentiviral vector and two packaging plasmids pCMV-VSV-G-RSV-Rev and pCAG-HIVgp using *Trans*IT-X2. The complex was added in HEK293T cells and incubated 3 days. After collection of HEK293T medium, CT26 was cultured with 1:1 mixture of HEK293T medium and fresh medium, following selection by puromycin.

Quantitative PCR analysis

Total RNA was extracted using TRIsure reagent (Bioline). cDNA was synthesized using ReverTra Ace® qPCR RT Master Mix (Toyobo). Quantitative PCR was performed on cDNA using KAPA SYBR® FAST qPCR Master Mix (2X) ABI Prism® (Kapa Biosystems) on a StepOnePlus Real-Time PCR System (Thermo Fisher Scientific). The primers are listed in Supplementary Table 2.

Cell viability assay

To assess cell viability, MTT assay was performed using MTT Cell count kit (Nacalai Tesque). Absorbance at a test wavelength of 570 nm and a reference wavelength of 650 nm was measured by using a Multiskan FC (Thermo Fisher Scientific). Cell proliferation was observed up to 4 days.

Enzyme-linked immunosorbent assay (ELISA)

The production of IL-34 in cell lines was measured with ELISA. Culture supernatants were collected at 48 h after seeding the cells at a density of 1×10^6 in 6-well plate. The IL-34 contents was measured with LEGEND MAX Mouse IL-34 ELISA kit with Pre-Coated Plates (Biolegend).

55

56 **Isolation of tumor-infiltrating immune cells from solid tumor**

57 Isolation of tumor-infiltrating immune cells from solid tumors was performed by using BD
58 Horizon™ Dri Tumor & Tissue (Becton, Dickinson, and Company). The recovered tumor-
59 infiltrating cells were used as samples for flow cytometry or RNA extraction.

60

61 **Flow cytometry**

62 Cells were washed and blocked with FcR Blocking Reagent (TONBO biosciences) and
63 stained with 4',6-diamidino-2-phenylindole (DAPI, Cayman Chemical Company) and the
64 antibodies against following molecules; CD3ε, CD4, CD8α, F4/80, CD11b, CD11c, CD45,
65 CD115, IA-IE (MHC class II), iNOS, Arginase 1 and PD-L1 (BioLegend). Data were
66 acquired using BD FACSCanto II, BD FACSAria, or BD FACSCelesta flow cytometer, and
67 analyzed using FlowJo software. Detailed information about antibodies is described in
68 Supplementary Table 1.

69

70 **Next-generation sequencing and data analysis**

71 Total RNA was extracted using PureLinkTM RNA Mini Kit (Life Technologies). Next-
72 generation sequencing was performed at Kazusa DNA Research Institute (illumina HiSeq

2500). The quality and concentration of the RNA was verified with Agilent 2100 Bioanalyzer and Quantus Fluorometer (Promega), respectively. All the samples showed RIN values > 8. Sequencing libraries were prepared using Agilent SureSelect Strand-Specific RNA Library Prep for Illumina according to the manufacturer's instructions. Briefly, poly-A RNA was purified from 300 ng total RNA per sample using oligo dT magnetic beads. The libraries were PCR amplified for 13 cycles and purified with AMPure XP beads. Sequencing of the libraries was conducted on the Illumina HiSeq2500 system performing paired-end 100 bp reads. The reads were mapped to mouse reference genome mm10 with Tophat (v2.1.0), and caluculated FPKM (fragments per kilobase of exon per million reads mapped) value with cufflinks (v2.2.1). The FPKM values were normalized by CD45, and shown as global z-score.

Immunohistochemistry staining

For DAB staining, immunohistochemistry staining was performed on paraffin-embedded tumor tissue sections. PD-L1 was stained using DAB (Dojindo) followed by hematoxylin conterstaining (Fujifilm Wako Pure Chemical Industries). PD-L1 staining was kindly performed by Dr. Yutaka Hatanaka, Research Division of Genome Companion Diagnostics, Hokkaido University Hospital. For multiple immunofluorescent staining, Opal

4-color fluorescent IHC kit (Perkin-Elmer) was used. Tumor sections were objectively judged by two independent researchers at 600× magnification for each section. More than 6 tumor areas in each section were randomly selected for evaluation. FV1000 OLYMPUS software was used for quantification of immunofluorescent staining. Detailed information about antibodies is described in Supplementary Table 1.

PDX model

PDX model was performed at DNA Link, Inc. Firstly, HuNSG mice were generated as previously reported by The Jackson Laboratory (Shultz et al., 2005). In brief, human fetal liver $CD34^+$-purified HSC were purchased from Stem Express and intravenously injected into three-week-old female NSG mice (10^5 cells/mouse), 4h post-140 cGy total body irradiation using the RS-2000 irradiator (Rad Source). The engraftment levels of human $CD45^+$ cells were determined 12 weeks post-HSC transplantation by flow cytometric quantification of peripheral blood. HuNSG mice that had over 25% of human $CD45^+$ cells in the peripheral blood were considered as engrafted and humanized. PDX models were generated using tumor tissues from patients who underwent surgery as the primary treatment strategy for lung cancer at Samsung Medical Center. Twelve weeks post-human HSC transplantation, 30-40 μl finely minced tumors were injected s.c. into the left flank of

HuNSG mice. Treatment was started when the tumor volumes reached 70-120 mm^3. Treatment with anti-human IL-34 (BioLegend; 250 μg per injection, 3 times a week for 4 weeks), anti-human PD-1 (Selleckchem; 10 mg/kg for the first dose, followed by 5 mg/kg dose every 5 days), antibodies combination, or saline was administered intraperitoneally. Vehicle control saline (Sigma Aldrich) was administered 3 times per week until the endpoint. Tumor size was measured by caliper twice a week, and volumes (mm^3) were calculated by (length×$width^2$)/2.

For histological analysis, tumor tissues were fixed with 4% formaldehyde, embedded with paraffin and sections were stained with hematoxylin and eosin.

All animal experiments were performed under the guidelines approved by the Institutional Animal Care and Use Committee of Seoul National University Biomedical Research Institute.

Statistics

Statistical analysis was perfomed with JMP® 14 (SAS Institute Inc.). Significance was determined by Student's *t*-test, Tukey's multiple comparison test, or Steel-Dwass nonparametric multiple comparison test. p-Value was considered statistically significant when < 0.05.

Supplemental Reference

Shultz, L.D., Lyons, B.L., Burzenski, L.M., Gott, B., Chen, X., Chaleff, S., Kotb, M., Gillies, S.D., King, M., Mangada, J., et al. (2005). Human Lymphoid and Myeloid Cell Development in NOD/LtSz- *scid IL2R* γ ^{null} Mice Engrafted with Mobilized Human Hemopoietic Stem Cells. J. Immunol. *174*, 6477–6489.

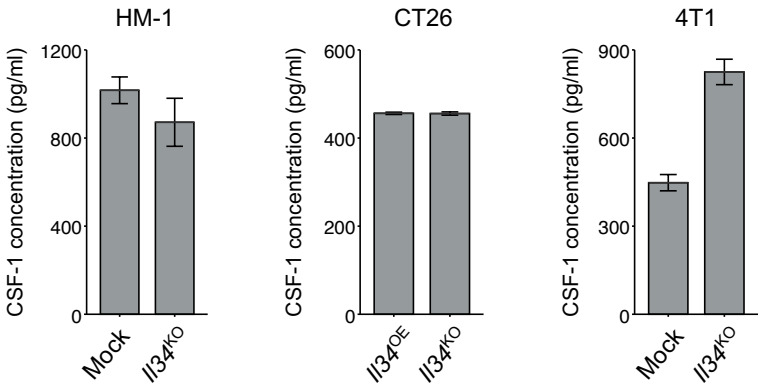

Figure S1 : The expression of CSF-1 from various murine cancer cell lines. Related to Figure 1, 2.

CSF-1 concentration in supernatants of HM-1, CT26 and 4T1 cell lines (n=3/cell line).

Data represent mean ± SEM.

Figure S1

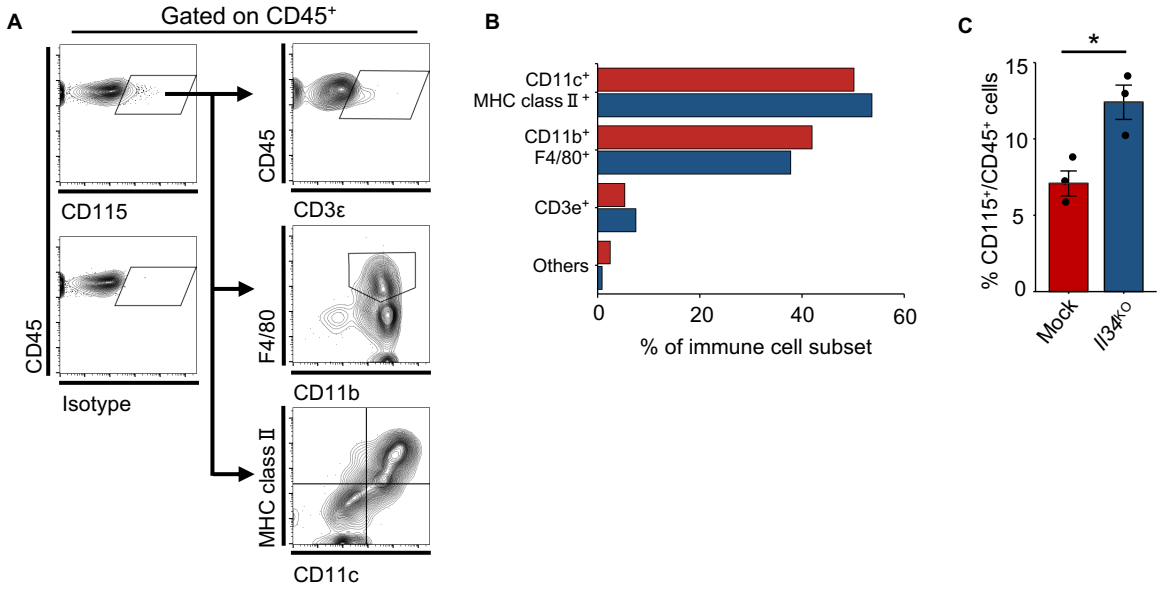

Figure S2 : Identification of the immune cell subset expressing CD115 in mock-HM-1 and *Il34*^{KO}-HM-1 tumors. Related to Figure 1.

(A) Representative flow cytometry profiles showing CD115+ cells within tumor-infiltrating CD45^{+} cells in HM-1 tumor.

(B) Bar graph shows the cell type expressing CD115 within tumor-infiltrating CD45^{+} cells (n=3/group).

(C) Bar graph represent the frequency of CD115^{+} cells within tumor-infiltrating CD45^{+} cells in mock- or *Il34* ^{KO}-HM-1 tumors (n=3/group). Data represent mean ± SEM. *p<0.05; two-tailed Student's t-test.

Figure S2

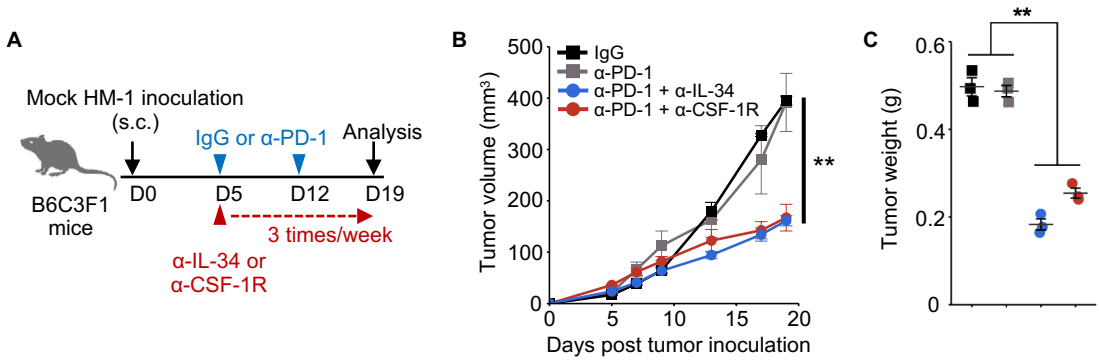

Figure S3 : IL-34 blockade equally enhanced anti-tumor efficacy of α-PD-1 treatment comparing with CSF-1R blockade in HM-1 model. Related to Figure 1.

(A) Schematic of the α-PD-1 mAb treatment in combination with α-IL-34 or α-CSF-1R mAb. The timeline shows the procedure of tumor inoculation and antibody treatment.

(B) Mock HM-1 tumor growth in B6C3F1 mice treated with the indicated antibodies (n=3-4/group).

(C) Tumor weight on day 19 after tumor inoculation (n=3-4/group).

Data represent mean ± SEM. **p<0.01; Tukey's multiple comparison test.

Figure S3

A *Il34*^{KO} vs. *Il34*^{OE} (treated by α-PD-1 mAb)

Canonical Pathway	p-value
T cell receptor signaling pathway	3.68E-10
Graft-versus-host disease	4.47E-10
Antigen processing and presentation	9.52E-10
Systemic lupus erythematosus	3.84E-09
Allograft rejection	5.42E-09
Asthma	3.76E-08
Cell adhesion molecules (CAMs)	3.86E-08
Hematopoietic cell lineage	1.05E-07
Type I diabetes mellitus	2.25E-07
Cytokine-cytokine receptor interaction	2.45E-07

Figure S4 : Clustering the gene expression data on NGS by Gene Ontology analysis. Related to Figure 2.

(A) The list of gene-set clusters enhanced in *Il34*^{KO} CT26 group compared to *Il34*^{OE} CT26 group.

(B) Heatmap shows the differentially of gene expression on selected several gene-set clusters.

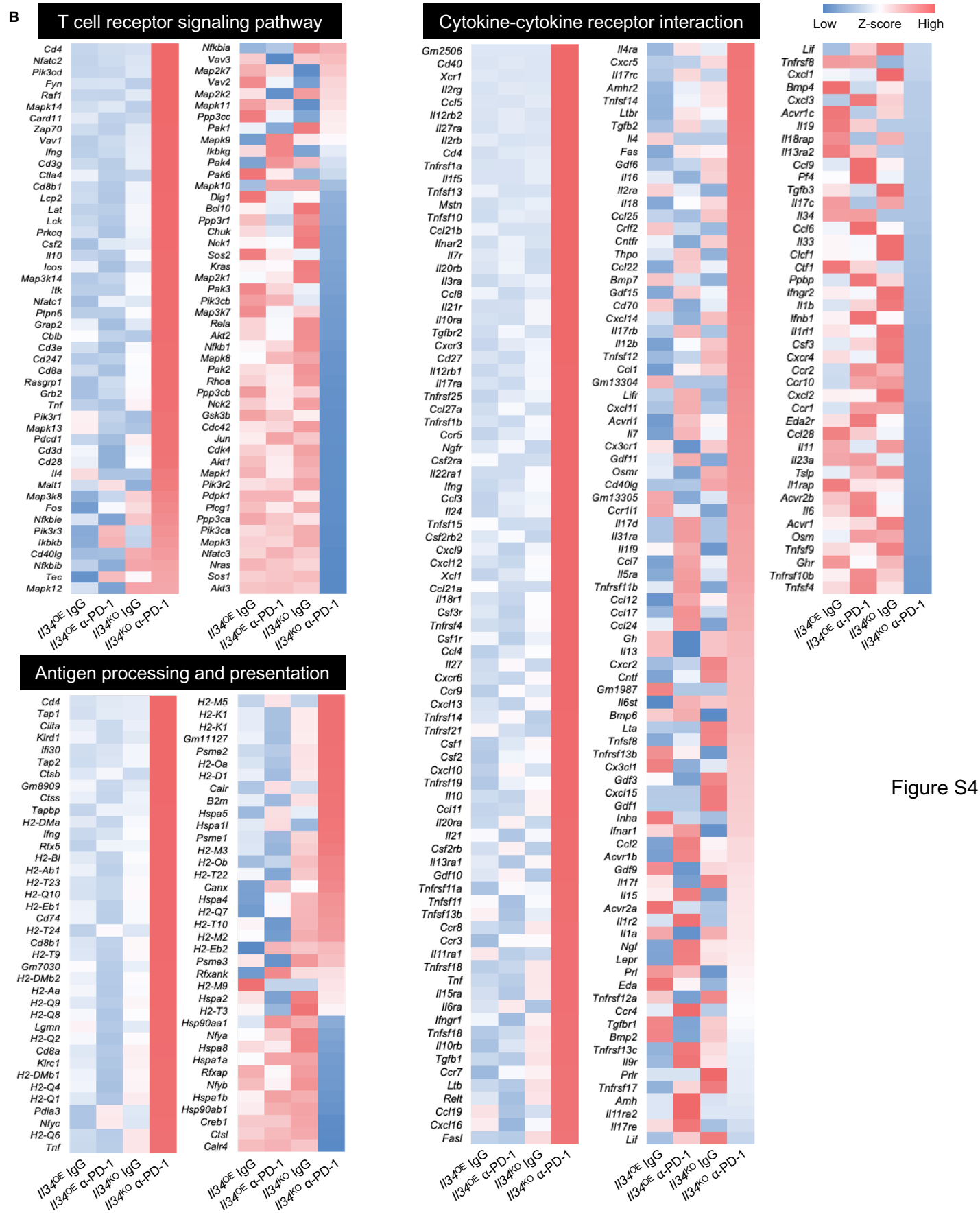

Figure S4

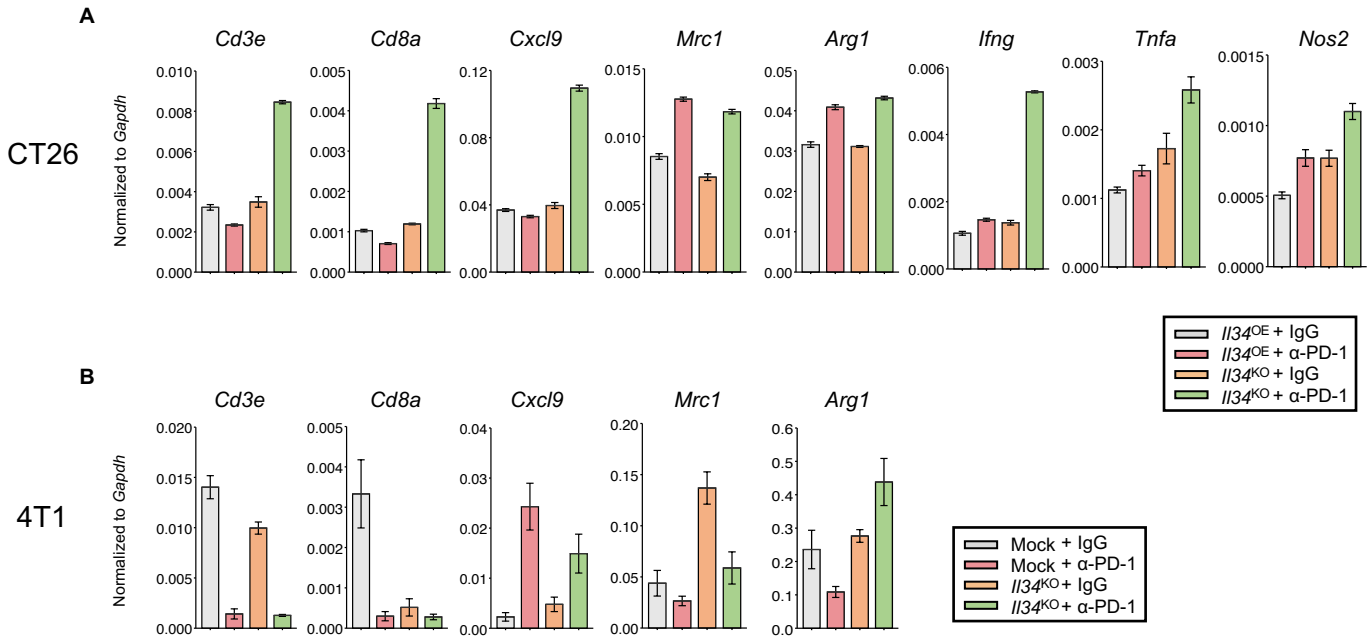

Figure S5 : qPCR analysis in CT26 and 4T1 tumors. Related to Figure 2.

(A) Expression of selected genes were evaluated by qPCR analysis in CT26 tumor samples used for NGS analysis (Fig. 2D).

(B) Gene expression displayed in (A) were analyzed by qPCR in 4T1 tumors (n=3/group).

Data represent mean ± SEM of technical triplicate.

Figure S5

Key resources table

REGENT & RESOURCE	SOURCE	IDENTIFIER
Antibodies		
Anti-mouse CD3ε (145-2C11) APC	BioLegend	Cat#100236; RRID: AB_2561456
Anti-mouse CD4 (RM4-5) APC-Cy7	BioLegend	Cat#00525; RRID: AB_312726
Anti-mouse CD8α (53-6.7) FITC	BioLegend	Cat#00706; RRID: AB_312745
Anti-mouse CD11b (M1/70) FITC	BioLegend	Cat#101206; RRID: AB_312789
Anti-mouse CD11c (N418) APC	BioLegend	Cat#117309; RRID: AB_313778
Anti-mouse CD45 (30-F11) Pacific blue	BioLegend	Cat#103126; RRID: AB_493535
Anti-mouse CD45 (30-F11) FITC	BioLegend	Cat#103108; RRID: AB_312973
Anti-mouse CD45 (30-F11) PE	BioLegend	Cat#103106; RRID: AB_312971
Anti-mouse CD45 (30-F11) APC	BioLegend	Cat#103112; RRID: AB_312977
Anti-mouse CD45 (30-F11) PE-Cy7	BioLegend	Cat#103114; RRID: AB_312979
Anti-mouse CD45 (30-F11) APC-Cy7	BioLegend	Cat# 103116; RRID: AB_312981
Anti-mouse F4/80 (BM8) APC	BioLegend	Cat#123116; RRID: AB_893481
Anti-mouse CD274 (MIH5) APC	BioLegend	Cat#124311; RRID: AB_10612935
Anti-mouse CD273 (TY25) PE	BioLegend	Cat#107205; RRID: AB_2299418
Anti-mouse CD80 (16-10A1) FITC	BioLegend	Cat#104705; RRID: AB_313126
Anti-mouse CD86 (GL-1) FITC	BioLegend	Cat#105005; RRID: AB_313148
Anti-mouse CD115 (AFS98) APC	BioLegend	Cat#125509; RRID: AB_2085222
Anti-mouse I-A/I-E (M5/114.15.2) FITC	BioLegend	Cat#107606; RRID: AB_313321
Anti-mouse iNOS (CXNFT) APC, eBioscience™	Invitrogen™	Cat#17-5920-80; RRID: AB_2573244
Anti-human/mouse Arginase 1 (A1exF5) PE, eBioscience™	Invitrogen™	Cat#12-3697-80; RRID: AB_2734839
Purified anti-mouse CD16/CD32 (2.4G2) (Fc Block)	TONBO bioscience	Cat#70-0161; RRID: AB_2621487
Purified anti-mouse CD45 (30-F11)	BioLegend	Cat#10302; RRID: AB_312967
Purified anti-mouse F4/80 (BM8)	BioLegend	Cat#123101; RRID: AB_893504
Purified anti-mouse Areginase-1 (D4E3M)	CST	Cat#93668; RRID: AB_2800207
Purified anti-mouse Nos2 (Rabbit polyclonal)	Abcam	Cat#ab15323; RRID: AB_301857
Purified anti-mouse PD-1 (RMP1-14)	Dr. Hideo Yagita (Juntendo University, Tokyo)	N/A

Purified anti-mouse CTLA-4 (UC10-4F10)	Dr. Hideo Yagita (Juntendo University, Tokyo)	N/A
Purified anti-mouse IL-34 (C054-35)	BioLegend	Cat#147202; RRID: AB_2563031
Purified anti-mouse CSF-1R (AFS98)	Bioxell	Cat#BE0213; RRID: AB_2687699
ChromPure Rat igG, whole molecule	Jackson Immuno Research LABORATPRIES, INC.	Cat#012-000-003; RRID: AB_2337136
Purified anti-human IL-34 (1D12)	Millipore	Cat#MABT493
Purified anti-human CD274 (E1L3N)	CST	Cat#13684; RRID: AB_2687655
Purified anti-human PD-1 (monoclonal)	Selleckcheme	Cat#A2002; RRID: AB_2810223
Purified anti-human IL-34 (E0320E7)	BioLegend	Cat#361302; RRID: AB_2563033
Cell Culture Regents		
RPMI-1640with L-Glutamine and Phenol Red	Fujifilm Wako Pure Chemical Industries	Cat#189-02025
D-MEM (high Glucose) with L-Glutamine and Phenol Red	Fujifilm Wako Pure Chemical Industries	Cat#044-29765
MEMα with L-Glutamine and Phenol Red	Fujifilm Wako Pure Chemical Industries	Cat#135-15175
Defined fetal bovine serum	Sigma Aldrich	Cat#F7524
Penicillin-Streptomycin Mixed Solution (100x)	Nacali Tesque	Cat#26253-84
MEM Non-Essential Amino Acid Solution (100x)	Nacali Tesque	Cat#06344-56
2.5g/l-Trypsin/1mmol/l-EDTA Solution, with Phenol Red	Nacali Tesque	Cat#32777-15
Critical Commercial Regents		
TransIT-X2® Dynamic Delivery System	Takara	Cat#V6104
LEGEND MAX™ Mouse IL-34 ELISA Kit	BioLegend	Cat#439107
eBioscience™ Fixation/Permeabilization Concentrate	Invitrogen™	Cat#00-5123-43
eBioscience™ Fixation/Permeabilization Diluent	Invitrogen™	Cat#00-5223-56
eBioscience™ Permeabilization Buffer (10X)	Invitrogen™	Cat#00-8333-56

BD Horizon™ Dri Tumor & Tissue Dissociation Reagent (TTDR)	BD bioscience	Cat#661563
Experimental Models: Cell Lines		
OV2944-HM-1	Japanese Collection of Research Bioresources	Cat#JCRB1208
CT26	Dr. Hidemitsu Kitamura (Hokkaido University, Hokkaido)	N/A
4T1	ATCC	Cat#CRL-2539
Experimental Models: Organisms/Strains		
B6C3F1	Japan SLC, Inc.	N/A
Balb/c	Japan SLC, Inc.	N/A
Plasmids		
pCAG-VSVG	Addgene	Cat#8454
pCMV-VSV-G-RSV-Rev	Addgene	Cat#35616
IL-34 CRISPR/Cas9 KO Plasmid (m)	Santa Cruz Biotechnology, Inc.	Cat#sc-429354
pLenti-EF1a-C-Myc-DDK-IRES-Puro	Origene	Cat#PS100085

Primer list for quantitative PCR analysis

Species	Gene	Forward (5'-3')	Reverse (5'-3')
Mouse	Gapdh	TCAAATGGGGTGAGGCCGGT	TTGCTGACAATCTTGAGTGA
	Cd3e	AAGTAATGAGCTGGCTGCGT	TCGTCACTGTCTAGAGGGCA
	Cd8a	GGATTGGACTTCGCCTGTGA	TGGGACATTTGCAAACACGC
	Mrc1	CTCTGTTCAGCTATTGGACGC	TGGCACTCCCAAACATAATTTGA
	Ifng	AAGACAATCAGGCCATCAGCA	AGCGACTCCTTTTCCGCTTC
	Tnfa	TTCTATGGCCCAGACCCTCA	CTTGGTGGTTTGCTACGACG
	Nos2	ACATCGACCCGTCCACAGTAT	CAGAGGGGTAGGCTTGTCTC
	Arg1	GTATGACGTGAGAGACCACG	CTCGCAAGCCAATGTACACG
	Cxcl9	AATGCACGATGCTCCTGCA	AGGTCTTTGAGGGATTTGTAGTG
	Cxcl10	AGTGCTG CCGTCATTTTCTG	TCCCTATGGCCCTCATTCTCA
	Cxcl11	GTAATTTACCCGAGTAACGGC	CACCTTTGTCGTTTATGAGCCTT